J|A|C|S
ARTICLES
Published on Web 08/29/2003

Potential-Dependent Reorientation of Thiocyanate on Au Electrodes

Xiao Li and Andrew A. Gewirth*

Contribution from the Department of Chemistry and Fredrick Seitz Materials Research Laboratory, University of Illinois at Urbana-Champaign, Urbana, Illinois 61801

Received May 23, 2003; E-mail: agewirth@uiuc.edu

Abstract: Thiocyanate (SCN) adsorption on an Au electrode is examined using surface-enhanced Raman scattering (SERS) measurements, along with detailed density functional theory (DFT) calculations. Both the calculation and the spectroscopic measurements show that three different geometries are adopted by SCN adsorption in the potential region studied ($0.0\ V \leq E \leq 1.2\ V$ vs NHE). At low potential both N-bound and S-bound forms are found, at intermediate potentials around the potential of zero charge (E_{pzc}) the S-bound form dominates, and at high potentials SCN associates with the Au surface via a bridging geometry. The Stark slope observed for the C−N stretch in the N- and S-bound forms is positive, while the bridge form exhibits a negative Stark slope. DFT calculations show that the potential-dependent reorientation of SCN arises from overlap of specific SCN-based orbitals with the Fermi level of the Au surface; as the Fermi energy changes, different orbital overlaps are found. The calculations also provide an explanation for the different signs of the Stark slope observed for different geometries. For the end-on adsorption, the lowest unoccupied molecular orbital (LUMO) associated with the C−N bond is antibonding, while the corresponding LUMO in the bridge form is bonding.

I. Introduction

The potential-dependent adsorption of halides and pseudohalides on metal surfaces has long been studied to elucidate features of the metal−adsorbate interaction and also to probe the interplay between metal, adsorbate, solvent, and electrolyte that constitutes the electrified solid−liquid interface.[1] The adsorption of thiocyanate (SCN) on metal surfaces is of particular interest because this molecule presents ambidentate functionality with the possibility of either N or S coordination. Potential-dependent studies of SCN on metal surfaces are of interest because changes in the adsorption geometry reflect changes in the electronic structure of the metal. In particular, there are two canonical forms for free SCN^-, as shown in eq 1:[2]

$$|S^- - C \equiv N| \leftrightarrow \langle S = C = N\rangle^- \qquad (1)$$

The nitrogen end of this ion is a hard base, while the sulfur end is a soft base. As a result, N-bonding is expected to form with a hard metal while S-bonding is preferred with a soft metal.

Thiocyanate has seen extensive use in electroplating baths[3] and is employed extensively for studies of ionic associations and interactions.[4] SCN forms bond with the metals via the S or N end,[5] via both ends in bridge form,[6] and also in three-way-bridging M_2SCN-M' geometry.[7]

Because of its strong adsorption on metal surface and the large infrared and Raman cross section of the C−N stretch, thiocyanate has been studied extensively by in situ vibrational spectroscopies[8−11] such as confocal microprobe Raman spectroscopy (CMR),[10] surface-enhanced Raman spectroscopy (SERS),[12] potential-difference infrared spectroscopy (PDIR),[13,14] polarization-modulation reflection absorption infrared spectroscopy (PM-RAIRS),[15] attenuated total internal reflection infrared spectroscopy (ATR),[16] and sum-frequency generation (SFG).[17,18] The frequency of the C−N stretch is sensitive to both the adsorption geometry and the electrode potential via the Stark effect. Generally, as potential increases, the adsorption geometry of SCN on the metal surfaces changes from N-bound to S-bound. On Au surfaces, SCN end-on adsorption has been reported in the potential range between −0.3 and 0.8 V vs NHE.[12] Interestingly, bridge adsorption of SCN has never been reported on an Au surface, but has been seen on Pt and Ni

(1) Magnussen, O. M. *Chem. Rev.* **2002**, *102*, 679−725.
(2) Tielens, F.; Saeys, M.; Tourwe, E.; Marin, G. B.; Hubin, A.; Geerlings, P. *J. Phys. Chem. A* **2002**, *106*, 1450−1457.
(3) Schlesigner, M.; Paunovic, M. *Modern Electroplating*, 4th ed.; John Wiley & Sons: New York, 2000.
(4) Bacelon, P.; Corset, J.; De Loze, C. *J. Solution Chem.* **1980**, *9*, 129−139.
(5) Schwerdtfeger, P.; Boyd, P. D. W.; Burrell, A. K.; Robinson, W. T.; Taylor, M. J. *Inorg. Chem.* **1990**, *29*, 3593−3607.
(6) Panattoni, C.; Frasson, E. *Acta Crystallogr.* **1963**, *16*, 1258.
(7) Gronbaek, R.; Dunitz, J. D. *Helv. Chim. Acta* **1964**, *47*, 1889−1897.
(8) Ashley, K.; Samant, M. G.; Seki, H.; Philpott, M. R. *J. Electroanal. Chem.* **1989**, *270*, 349−364.
(9) Cao, P.; Yao, J.; Ren, B.; Gu, R.; Tian, Z. *J. Phys. Chem. B* **2002**, *106*, 7283−7285.
(10) Ren, B.; Huang, Q.-J.; Xie, Y.; Tian, Z.-Q. *Anal. Sci.* **2000**, *16*, 225−234.
(11) Bron, M.; Holze, R. *Electrochim. Acta* **1999**, *45*, 1121−1126.
(12) Corrigan, D. S.; Foley, J. K.; Gao, P.; Pons, S.; Weaver, M. J. *Langmuir* **1985**, *1*, 616−620.
(13) Corrigan, D. S.; Gao, P.; Leung, L. W. H.; Weaver, M. J. *Langmuir* **1986**, *2*, 744−752.
(14) Gao, P.; Weaver, M. J. *J. Phys. Chem.* **1986**, *90*, 4057−4063.
(15) Samant, M. G.; Kunimatsu, K.; Viswanathan, R.; Seki, H.; Pacchioni, G.; Bagus, P. S.; Philpott, M. R. *Langmuir* **1991**, *7*, 1261−1268.
(16) Parry, D. B.; Harris, J. M.; Ashley, K. *Langmuir* **1990**, *6*, 209−217.
(17) Ong, T. H.; Davies, P. B.; Bain, C. D. *J. Phys. Chem.* **1993**, *97*, 12047−12050.
(18) Williams, C. T.; Yang, Y.; Bain, C. D. *Langmuir* **2000**, *16*, 2343−2350.

10.1021/ja0363112 CCC: $25.00

surfaces at very high potentials (E > 1.2 V vs NHE).[10,19] Correlation of different adsorption geometries with surface electronic structure remains to be established.

In this paper we utilize SERS to examine the adsorption of SCN on Au surfaces. The advantage of SERS is that it can probe dipoles oriented both parallel and perpendicular to the metal surface, a feature not found with the stricter selection rules attendant IR or SFG spectroscopies. However, this advantage comes with a corresponding cost in that SERS studies are performed on a roughened surface, and the exact site of the SERS response remains unclear.[20,21] This aspect of SERS may complicate the connection between the spectroscopic features and exact surface structures. However, vibrational spectroscopy is clearly a sensitive probe of SCN adsorption geometry. In the complexes, the C−N stretching mode generally has a sequence of bridge > SCN^- > NCS^-.[22] N-bound usually leads to a little or even negative frequency shift in the C−N stretch relative to free ion value at around 2057 cm^{-1},[23] while the S-bound results in an increase to around 2100 cm^{-1}, depending on the nature of the metal ion. It has been observed that the bridging bound is well above 2100 cm^{-1}.[22]

Ab initio calculations have been widely applied to molecule−surface systems over the last few decades.[24] Compared with the cluster-based methods and embedded-adsorbate method (EAM), the supercell calculations used in this paper feature faster convergence and excellent agreement with experimental results.[25] Recently, successful calculations of this type have been performed between a series of small molecules and metal surfaces,[26] and we have recently used these to examine the interaction between peroxide and modified Au surfaces.[27] Detailed calculations of free thiocyanate structure and vibrational modes have been performed and give reasonable results compared with experiment.[28] However, the only calculations examining the adsorption of SCN on a metal surface have been restricted to end-on adsorption of SCN on an Ag cluster model.[2,29] The work of Geerlings et al. suggested the occurrence of N-bound SCN at positive potentials, a prediction which has not been verified experimentally.[2]

In this paper, we use SERS to investigate SCN adsorption on an Au surface over the potential range of 0.0−1.2 V vs NHE, in conjunction with detailed ab initio calculations examining the interaction between SCN and Au at different potentials. We address the electronic structural origin of changes in the SCN adsorption geometry as a function of potential, the origin of different signs of the Stark shift occurring with different adsorption geometries, and evaluate different SCN adsorption geometries at high potentials.

II. Methodology

All solutions were prepared from ultrapure water (Milli-Q UVplus, Millipore, Inc.; 18.2 MΩ cm). Reagent-grade KSCN (Alfa Asar) and $HClO_4$ (70%, Baker, UltrexII) were used for preparing solutions. Cyclic voltammograms were obtained in a glass electrochemical cell using an AFRDE5 (Pine Instrument Co.) potentiostat. The polycrystalline gold was first annealed for 3 min in a hydrogen flame and quenched by ultrapure water. A gold wire (Alfa, 99.9985%, 0.5 mm in diameter) was used as the counter electrode. Ag/AgCl electrode was used as the reference. All potentials were reported with respect to NHE in this paper. Au single crystals were obtained from Monocrystals and were prepared as described previously.[30]

Au crystal preparation, cyclic voltammogram, and SERS instrumentation have been described previously.[27] Spectra were obtained between 150−2700 cm^{-1} at 0.1 V intervals. The system was allowed to equilibrate for 2 min at each potential before acquiring spectra. The spectral resolution was estimated to be 3 cm^{-1}. The baseline for each SERS spectrum was corrected prior to presentation. The concentration of SCN was 1.7 μM in these measurements.

Calculations on periodic structures were carried out using CASTEP in MSI−Cerius[2].[31] Density function theory calculations with the generalized gradient approximation (GGA) were performed. Ultrasoft pseudopotentials were used to describe the electron−core interactions. Valence states included the 5d and 6s shells for Au, 3s and 3p for S, and 2s and 2p for C and N atoms. The recent successful use of C and S pseudopotentials in the calculation of the adsorption of methyl thiolate on Au(111) shows that they should have utility here.[32] The electronic wave functions were expanded in a plane-wave basis set with an energy cutoff of 400 eV.[33] For total energy calculations, a Monkhorst−Pack k-point sampling scheme with 12 k-points in the super cell was applied. In this work, the Au(111) surface was modeled by a $p(2 \times 2)$ unit cell consisting of three layers and 12 Au atoms. The vacuum region between slabs was 10 Å. In all cases, surface modifications were applied to only one face of the slab. For SCN adsorption on the Au(111) surface, the topmost gold layer was allowed to relax during the geometry optimization process, while the other atoms were constrained in their position to mimic the bulk crystal. During single-point energy calculations, all the atom positions were fixed. Calculations for isolated ions or molecules were performed in the same supercell arrangement as above. Calculations were performed using an SGI Origin 2000 computer at the National Center for Supercomputing Applications (NCSA).

III. Results and Analysis

The cyclic voltammogram of SERS-active Au in 0.1 M $HClO_4$ solution with and without 1.7 μM KSCN in the region between 0.0 and 1.2 V is shown in Figure 1a. The current is mostly capacitive in this region, although the onset of Au oxidation can be discerned at the most positive potentials. The addition of KSCN has little effect on the electrochemical behavior of Au in this potential region. The only difference is in the Au oxidation region (E > 1.1 V) where the oxidation current decreases approximately 40% in the presence of KSCN. This voltammetry is consistent with that reported previously, albeit over a much wider potential range.[34]

(19) Tian, Z. Q.; Ren, B.; Mao, B. W. *J. Phys. Chem. B* **1997**, *101*, 1338−1346.
(20) Garrell, R. L. *Anal. Chem.* **1989**, *61*, 401A−411A.
(21) Weaver, M. J. *J. Raman Spectrosc.* **2002**, *33*, 309−317.
(22) Bailey, R. A.; Kozak, S. L.; Michelsen, T. W.; Mills, W. N. *Coord. Chem. Rev.* **1971**, *6*, 407−445.
(23) Gans, P.; Gill, J. B.; Fearnley, D. P. *J. Chem. Soc., Dalton Trans.* **1981**, 1708−1713.
(24) Over, H.; Tong, S. Y. In *Handbook of Surface Science*; Holloway, S., Richardson, N. V., Eds.; Elsevier: Amsterdam, 1996; Vol. 1, pp 425−502.
(25) Brivio, G. P.; Trioni, M. I. *Rev. Mod. Phys.* **1999**, *71*, 231−265.
(26) Lundqvist, B. I.; Bogicevic, A.; Carling, K.; Dudiy, S. V.; Gao, S.; Hartford, J.; Hyldgaard, P.; Jacobson, N.; Langreth, D. C.; Lorente, N.; Ovesson, S.; Razaznejad, B.; Ruberto, C.; Rydberg, H.; Schroder, E.; Simak, S. I.; Wahnstrom, G.; Yourdshahyan, Y. *Surf. Sci.* **2001**, *493*, 253−270.
(27) Li, X.; Gewirth, A. A. *J. Am. Chem. Soc.* **2003**, *125*, 7086−7099.
(28) Schultz, P. W.; Leroi, G. E.; Harrison, J. F. *Mol. Phys.* **1996**, *88*, 217−246.
(29) Pacchioni, G.; Illas, F.; Philpott, M. R.; Bagus, P. S. *J. Chem. Phys.* **1991**, *95*, 4678−4684.
(30) Angerstein-Kozlowska, H.; Conway, B. E.; Hamelin, A.; Stoicoviciu, L. *J. Electroanal. Chem.* **1987**, *228*, 429−453.
(31) *Cerius2*, version 4.8; Accelrys Inc.: San Diego, CA, 2002.
(32) Gottschalck, J.; Hammer, B. *J. Chem. Phys.* **2002**, *116*, 784−790.
(33) Yourdshahyan, Y.; Zhang, H. K.; Rappe, A. M. *Phys. Rev. B* **2001**, *63*, 1405.
(34) Walters, M. J.; Pettit, C. M.; Bock, F. X.; Biss, D. P.; Roy, D. *Surf. Interface Anal.* **1999**, *27*, 1027−1036.

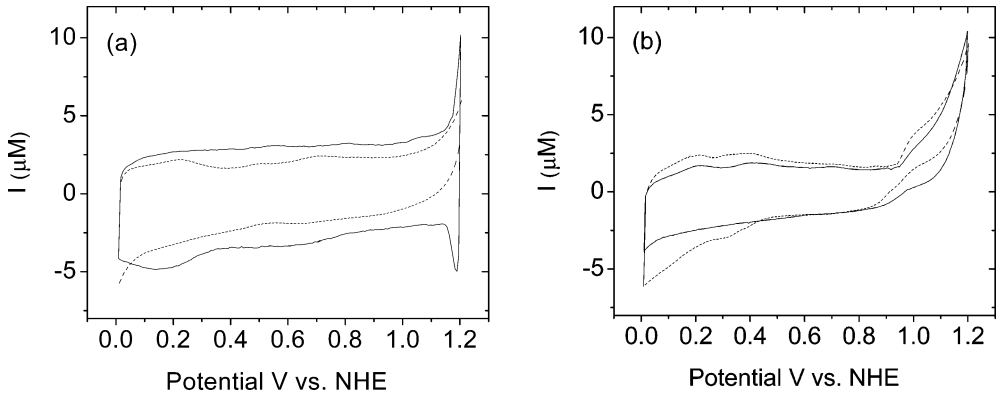

Figure 1. (a) Cyclic voltammogram of SERS active Au(poly) in 0.1 M $HClO_4$ (solid line) and 1.7 μM KSCN + 0.1 M $HClO_4$ (dotted line) solution. (b) CV in 1.7 μM KSCN + 0.1 M $HClO_4$ solution on Au(111) (solid line) and Au(100) (dotted line). The scan rate is 25 mV/s.

To evaluate the effect of using a polycrystalline material required for the SERS measurement, we examined the cyclic voltammogram of Au(111) and Au(100) single crystals in a solution containing 1.7 μM KSCN + 0.1 M $HClO_4$. These voltammograms are shown in Figure 1b. The electrochemical behavior of the single-crystal surfaces is very similar to that seen with the SERS-active Au electrode. All surfaces exhibit only a capacitive current within the potential region examined here and an asymmetric current in the Au oxidation region. The similarity of the CV measurements between these different surfaces suggests that substantial similarity exists between the single crystals and polycrystalline systems.

III.A.1. SERS Spectra with KSCN. Shown in Figure 2 are spectra obtained between 0.0 and 1.2 V in the presence of 1.7 μM KSCN. Two wavenumber regions are shown: between 400 and 500 cm^{-1} and between 2000 and 2300 cm^{-1}.

In Figure 2a, a peak at 455 cm^{-1} is found (peak 1) which is associated with the bending mode of NCS, δ(NCS).[14] Peak 1 is observed only at potentials positive of 0.9 V, and its intensity increases with increasing potentials. As the potential sweeps to more negative values, the peak intensity decreases. Below 0.9 V, peak 1 weakens, and it eventually disappears around 0.2 V.

In his study of SCN absorption on Au, Weaver reported additional features at 237, 295, and 705 cm^{-1}, which were associated with Au−S, Au−N, and C−S stretching modes, respectively.[14] We also observe the 237 and 295 cm^{-1} modes, with the same potential dependence reported previously (data not shown). We never saw the 705 cm^{-1} band, which might relate to differences in surface preparation or other factors.

Figure 2b shows SERS obtained from the 2000 to 2300 cm^{-1} spectral region. In this region, three peaks labeled 2, 3, and 4 are observed. Peak 3 around 2120 cm^{-1} is well-known to be the C−N stretching mode of SCN^-, which is adsorbed on the Au surface through the S atom, ν_{Au-SCN}(C−N).[13] This peak is present throughout the potential region studied, in agreement with previous work.[13]

Between 0.0 and 0.4 V during the anodic scan, a shoulder around 2090 cm^{-1}, peak 2, is observed. It weakens as potential is scanned to more positive values and disappears about 0.8 V. Upon the reverse potential scan, peak 2 reappears at about 0.4 V and becomes a distinct peak at 2063 cm^{-1} at 0.0 V. Since the frequency of peak 2 shifts to higher values as the potential increases, it is not likely associated with solution SCN^- which exhibits ν(C−N) around 2057 cm^{-1},[23] but rather with moieties on the surface. Infrared studies show that the C−N stretching mode of N-bound NCS^- to Au, ν_{Au-NCS}(C−N), is around 2050−2080 cm^{-1}.[22] Furthermore, it was suggested by Subtractively Normalized Interfacial Fourier Transform Infrared Spectroscopy (SNIFTIRS) that N-bound thiocyanate forms on the Au surface with a 2060 cm^{-1} mode at negative potentials.[12] Thus, it is reasonable to assign peak 2 to be the ν_{Au-NCS}(C−S) mode. The disappearance of peak 2 at more positive potentials suggests that thiocyanate progressively reorients from the N-bound to the S-bound form on the Au surface as the potential moves to positive values, as has been discussed previously.[35]

Above 0.8 V, peak 4 appears at 2210 cm^{-1}, and its intensity increases dramatically with potential. In the cathodic scan above 1.1 V, peak 4 continues to increase in intensity while peak 3 weakens simultaneously. Below 1.0 V, the intensity of peak 4 begins to drop slowly, but it remains strong even at 0.0 V. Holding the potential at 0.0 V for 2 h ultimately results in the disappearance of peak 4 and the recovery of peak 3. Alternatively, peak 3 can be recovered by holding the potential at −0.9 V for 20 min, followed by potential excursion to 0.0 V. This behavior implies that SCN^- adsorbs on the Au surface in a different geometry at high potential (E > 0.9 V), and this geometry only slowly reverts to the S-bound form indicated by peak 3.

In other measurements, we first applied potential at 0.8 V after equilibrating the electrode at open circuit. As shown in the Supporting Information, peaks 3 and 4 were seen. Stepping the potential to more negative values led to the loss of intensity in peak 4.

We next assign peak 4. No mode at such a high frequency has been reported previously for SCN^- on Au. As discussed in the Introduction, there are three different ways in which SCN can associate with a metal surface: bridging, N-bound, and S-bound. The CN stretch for these different geometries usually follows the order bridge > S-bound > N-bound.[36] Bridging SCN on Pt exhibits a C−N frequency of 2199 cm^{-1},[19] while that on Ni occurs at 2186 cm^{-1}.[10] Both of these are lower than the 2210 cm^{-1} value found here, while the C−N stretch for S-bound SCN on Au occurs at a higher frequency than the corresponding mode on Pt (2120 vs 2110 cm^{-1}). The occurrence of peak 4 at 0.8 V, negative of the potential of oxide formation on the Au surface, shows that Au oxide formation is not involved in the appearance of peak 4. Thus, we assign peak 4 to the C−N stretch of

(35) Bewick, A.; Pons, S. *Adv. Infrared Raman Spectrosc.* **1985**, *12*, 1−63.
(36) Bailey, R. A.; Michelsen, T. W.; Mills, W. N. *J. Inorg. Nucl. Chem.* **1971**, *33*, 3206−3210.

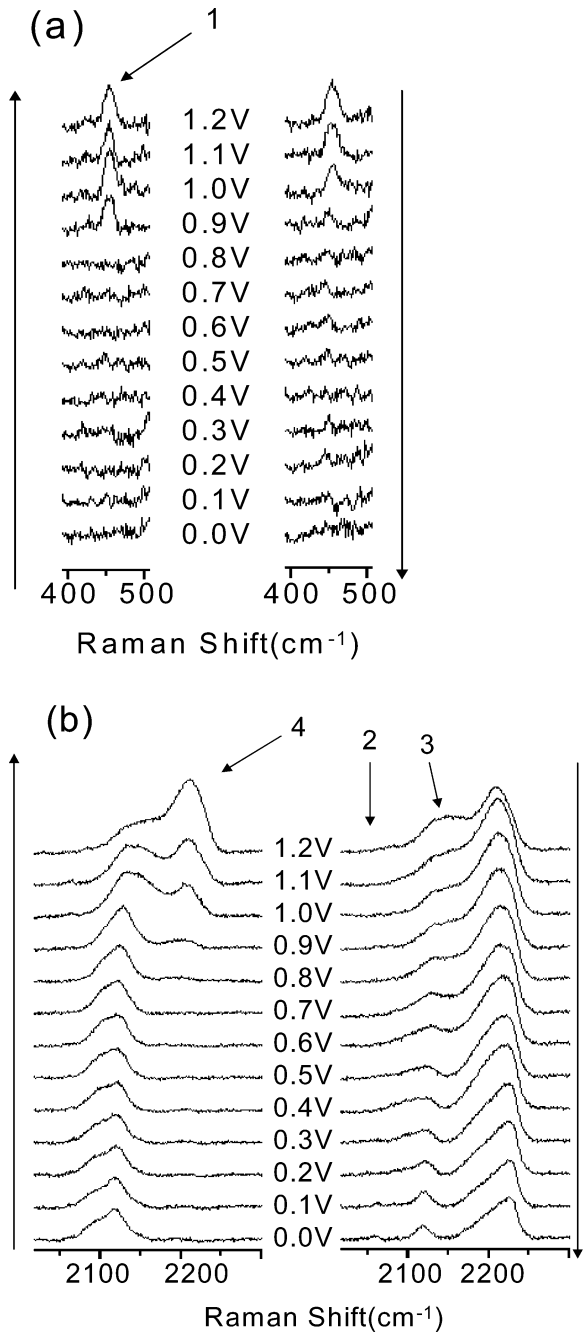

Figure 2. SERS spectra on Au(poly) in 1.7 μM KSCN + 0.1 M $HClO_4$ solution in two different spectral regions. The anodic potential sweep from 0 to 1.2 V is shown on the left of each panel, while the cathodic sweep is shown on the right.

bridge form SCN, $\nu_{Au-SCN-Au}$(C−N). This is the first time that an Au−SCN−Au adsorption geometry has been observed.

III.A.2. Potential Dependence of Bands 3 and 4. The frequencies of peaks 2, 3, and 4 all shift as the potential changes, which derives from the electric field (Stark) effect.[37] Figure 3 shows this behavior for peaks 3 and 4.

The Stark shifts for both peak 3 and peak 2 (data not shown) are positive. Figure 3a shows that the potential dependence of peak 3 can be divided into two segments: a low potential segment with $d\nu_{CN}/dE = 12.5$ cm^{-1} V^{-1} from 0.0 to 0.8 V and a high potential segment with $d\nu_{CN}/dE = 30$ cm^{-1} V^{-1} from 0.8 to 1.2 V. The former agrees well with the 12 cm^{-1} V^{-1} value quoted by Weaver between −0.3 and 0.7 V.[14] The higher value of $d\nu_{CN}/dE$ in the more positive potential region, which has not been observed before, must reflect a larger electric field experienced by the C−N group.

Figure 3b shows the frequency dependence on potential for ν(C−N) in the bridging geometry obtained after initially reaching a potential of 1.2 V. Interestingly, in both the cathodic scan and the following anodic scan, the Stark shift is *negative* and exhibits a value of −15 cm^{-1} V^{-1} within the potential region studied. There is one report of a negative Stark shift for the metal C stretch for CO on Pt and Ir surfaces.[38,39] However, this is the first time a negative Stark shift for a molecular-based vibrational mode has been reported. The origin of the negative Stark slope will be discussed later.

The potential dependence of ν(C−N) in the bridging geometry is less clear in the initial anodic scan prior to reaching 1.2 V. Here a positive Stark shift is seen, which then reverts to the negative slope described above on the subsequent cathodic scan (data not shown). Because the anodic and cathodic scans all follow the same slope in subsequent scans, we attribute this initial behavior to a kinetic effect, arising from the slow conversion of the S-bound SCN to the bridge-bound form.

III.B.1. Calculation Results for Bare Au(111). As a first test of the accuracy of our calculations, we computed the bulk and surface structural properties of Au(111). Figure 4 shows the (2 × 2) unit cell used to model the Au(111) surface. The blue line outlines the (2 × 2) unit cell. The calculation optimized the geometry of the bare Au slab by minimizing the total energy. The calculated lattice constant, $a_0 = 4.03$ Å, and the surface energy, $\gamma = 1188$ erg/cm^2, match well with the corresponding experimental values, $a_0 = 4.08$ Å and $\gamma = 1045-1410$ erg/cm^2.[40]

Previous efforts directed at simulating the effect of potential on adsorbate-electrode systems have been restricted to cluster-type calculations. The potential is simulated either by applying an external electric field[41−43] or by adding charge to the system.[2,42,44,45] In the CASTEP program used here, an external charge can be added, and charge neutrality is maintained by imposing a uniform counterbalancing background charge. Of course, this uniform background charge is not exactly representative of the physical situation at an electrode surface. Ideally, the surface charge on the electrode should be countered by a distant charge above the surface, and the surface charge would also be screened by electrolytes in close approach to the surface. This describes the physical situation in the electrochemical double layer. Alternatively, changing the charge state of the slab does give rise to a change in the Fermi energy as expected. We can use this change in Fermi energy to model a change in potential, as we show below. While the change in Fermi energy approach works well to model adsorbates interacting strongly with the surface, this approach will be less successful in the ultimate calculation of the electrochemical double layer.

(37) Lambert, D. K. *Solid State Commun.* **1984**, *51*, 297−300.
(38) Zou, S.; Weaver, M. J. *J. Phys. Chem.* **1996**, *100*, 4237−4242.
(39) Zou, S.; Gomez, R.; Weaver, M. J. *Langmuir* **1997**, *13*, 6713−6721.
(40) Cosandey, F.; Madey, T. E. *Surf. Rev. Lett.* **2001**, *8*, 73−93.
(41) O'Keeffe, J.; Wei, C.; Cho, K. *Appl. Phys. Lett.* **2002**, *80*, 676−678.
(42) Wasileski, S. A.; Weaver, M. J. *J. Electroanal. Chem.* **2002**, *524−525*, 219−230.
(43) Koper, M. T. M.; van Santen, R. A.; Wasileski, S. A.; Weaver, M. J. *J. Chem. Phys.* **2000**, *113*, 4392−4407.
(44) Engler, C.; Hofmann, A. *Z. Phys. Chem. (Munich)* **2001**, *215*, 461−482.
(45) Legault, M. D.; Bacelo, D. E. *J. Phys. Chem. A* **2002**, *106*, 9059−9064.

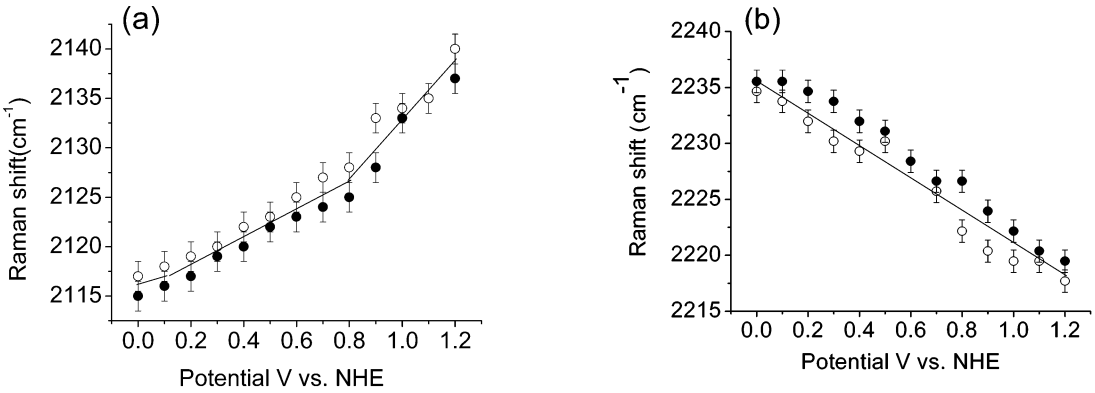

Figure 3. Potential dependence of SERS spectra frequency of (a) peak 3 ν_{Au-SCN}(CN) and (b) peak 4 $\nu_{Au-SCN-Au}$(CN) in solution containing 1.7 μM KSCN, 0.1 M$HClO_4$ on Au(poly). Filled and open circles represent the anodic and cathodic scan from 0.0 to 1.2 V, respectively.

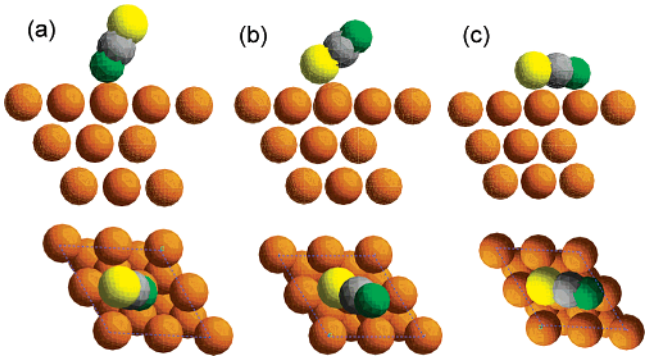

Figure 4. Side (top row) and top (bottom row) views of SCN adsorption on the Au(111) surface: (a) the N end-on adsorption with −1 e charge, (b) the S end-on adsorption with 0 e charge, and (c) the flat adsorption via both N and S ends with 1 e charge. Au, S, C, and N atoms are represented by orange, yellow, gray, and green circles, respectively.

As the software we use does not allow for addition of partial charge, geometry optimizations of the Au(111) slab with −1 e (addition of one electron) and +1 e (removal of one electron) external charges were performed. The calculated energy of the Fermi level of the slab changes from −5.920 and −6.742 to −7.763 eV, as the external charge increases from −1 e to 0 e to 1 e. The electrode potential E (V) is related to the work function, Φ (eV), as follows:[46−48]

$$E = \Phi/\mathrm{e} - E_\mathrm{k} \qquad (2)$$

E_k is the so-called absolute potential of the reference electrode used in the electrochemical measurements, and e is the charge on an electron. Here, the E_k is 4.6 V for the NHE electrode. Φ is defined as[49]

$$\Phi = \mathrm{e}V_\mathrm{ex} + \mathrm{e}V_\mathrm{dip} - E_\mathrm{fermi} \qquad (3)$$

where V_ex is the potential due to coupling between valence electrons, the bulk electron density, V_dip, is the surface-charge potential that an electron has to overcome to escape the surface, and E_fermi is the Fermi energy. While the exact values of V_ex and V_dip may be unknown, they are assumed to be constant with addition or subtraction of an electron. By combining eq 2 and 3, we obtain the relationship between the change in electrode potential and the change in Fermi energy:

$$\Delta E = \Delta E_\mathrm{fermi}/\mathrm{e} \qquad (4)$$

Table 1. SCN Calculation with Different Charges[a]

property/charge (e)	−1	0	1
$-E$ (eV)	709.440	705.039	694.660
S−C (Å)	1.631 (1.65)	1.596	1.566
C−N (Å)	1.192 (1.17)	1.198	1.221
q_S (e)	−0.39	0.26	0.85
q_C (e)	0.02	0.05	0.13
q_N (e)	−0.63	−0.31	0.02

[a] Values in parentheses are experimental results from ref 51.

To assign an experimentally relatable potential to the calculated Fermi energies, we associate the zero-charge calculation with the experimentally derived potential of zero charge (E_pzc). E_pzc for Au(111) in 0.1 M $HClO_4$ is measured to be 0.526 V (vs NHE).[50] With this value, the potential is estimated to be −0.30 V for −1 e charge and 1.55 V for +1 e charge.

Increasing charge on the slab results in small changes in the lattice constant. As the charge on the slab ranges from +1 to 0 to −1, the lattice constant increases from 3.95 to 4.03 to 4.23 Å, which can be explained by the increasing electron repulsion in the slab. We note that at negative potentials the Au(111) surface is observed to reconstruct; the slab size is not large enough in the present calculations to observe this behavior.

III.B.2. Calculation Results for SCN. To examine the effect of charge on the SCN moiety, we report the results of calculations for free SCN with different charges in Table 1. The table shows that as the charge changes from −1 to +1, the calculated total energy becomes less negative, indicating that SCN is more stable as an anion. With a charge of −1 on the molecule, the calculated S−C and C−N bond lengths of 1.631 and 1.192 Å, respectively, agree well with the experimental values of 1.65 and 1.17 Å.[51] Calculations on XCN^- (X = S, C, and Se) anions have been reported,[28] and our results for bond lengths in SCN match these predictions well. However, the reported charges on the S, C, and N atoms[28] differ somewhat from those we obtained by using a Mulliken population analysis, which is likely due to the different basis set and charge analysis

(46) Battaglin, C.; Carnera, A.; Mazzoldi, P.; Lodi, G.; Bonora, P.; Daghetti, A.; Trasatti, S. *J. Electroanal. Chem.* **1982**, *135*, 313−319.
(47) Trasatti, S. *Surf. Sci.* **1995**, *335*, 1−9.
(48) Trasatti, S. *J. Electroanal. Chem.* **1992**, *329*, 237−246.
(49) McCash, E. M. *Surface Chemistry*; Oxford University Press: New York, 2001.
(50) Hamm, U. W.; Kramer, D.; Zhai, R. S.; Kolb, D. M. *J. Electroanal. Chem.* **1996**, *414*, 85−89.
(51) Wells, A. F. *Structural Inorganic Chemistry*, 5th ed.; Oxford University Press: New York, 1983.

Table 2. Adsorption Energies[a] Calculated for SCN on Au with Different Charges (q)

charge (e)/geometry	Au–NCS[b]	Au–SCN[b]	Au–SCN–Au[c]
−1	−1.109	−1.105	1.984
0	−0.837	−1.187	−0.543
1	−0.459	−1.608	−3.062

[a] Adsorption energy is calculated from: $E_{ad} = E_{SCN/Au(111)}{}^{q} - E_{Au(111)}{}^{q} - E_{SCN}$. [b] Adsorbed end-on top site. [c] Adsorbed flat on the surface.

algorithm used.[52] However, the reported trends match our results well.

As the charge on SCN becomes more positive, the S−C bond length decreases considerably with a small increase in the C−N bond length. The origin of this behavior lies in the electronic configuration of SCN^-, which is $1\sigma^2 2\sigma^2 3\sigma^2 4\sigma^2\ 1\pi^4 2\pi^4$. Here the 1σ, 2σ, and 1π orbitals are primarily bonding, and the 3σ, 4σ and 2π orbitals are antibonding.[28] As the positive charge increases and electrons are removed from the antibonding 2π orbital (which has a major contribution from S and a smaller contribution from N [28]), the S−C bond length becomes shorter. The calculated Mulliken charges also suggest that the charge difference between the C and N atom decreases as the charge on SCN becomes more positive.

III.B.3. Calculation Results for SCN on Au(111). As the next step in evaluating the thiocyanate adsorption on the Au(111) surface, we added SCN to the Au(111) slab described above. Even though thiocyanate is stable in solution as an anion, SCN was used since the Au surface is an excellent source and sink of electrons.[29] There is little direct evidence concerning the structure adopted by SCN on Au(111), despite attempts using ex situ STM.[53] Alternatively, it is found that the SCN adsorption on Au follows a Langmuir isotherm, with coverage ranging between $\theta = 0.12-0.18$, depending on the potentials.[34] SCN adopts a (2×2) adlayer structure, with $\theta = 0.5$ on the Pt(111) surface[54,55] while $\theta = 0.25$ is on the Rh(111) surface.[56] To facilitate modeling, we chose to use one SCN adsorbed on a (2×2) Au(111) slab with a coverage of $\theta = 0.25$. There is no indication in the experimental results referenced above of cooperative behavior on Au. The similarity found between the voltammetry from the polycrystalline SERS-active material and the Au(111) surface shown in Figure 1 strongly supports the use of the Au(111) slab calculation to model the behavior observed in the SERS measurement.

III.B.3.(1). Potential Dependence of SCN Adsorption on Au(111). To evaluate the effect of potential on the adsorption geometry adopted by SCN on the Au(111) surface, we performed calculations using the three different geometries (N-bound, S-bound, and bridging) with each different charge. Table 2 shows the adsorption energy comparison for the three adsorption geometries at different external charges. Figure 4 shows the optimized geometries for each potential. For each charge a particular structure was found to be most stable by optimization, and the energies associated with the other two geometries were calculated by fixing the geometry in the desired configuration.

(52) Gross, K. C.; Seybold, P. G.; Hadad, C. M. *Int. J. Quantum Chem.* **2002**, *90*, 445−458.
(53) McCarley, R. L.; Kim, Y. T.; Bard, A. J. *J. Phys. Chem.* **1993**, *97*, 211−215.
(54) Peng, Q.; Breen, J. J. *Electrochim. Acta* **1998**, *43*, 2619−2626.
(55) Yau, S.-L.; Kim, Y.-G.; Itaya, K. *Anal. Sci. Technol.* **1995**, *8*, 723−730.
(56) Wan, L.-J.; Yau, S.-L.; Itaya, K. *J. Solid State Electrochem.* **1997**, *1*, 45−52.

Table 3. SCN Adsorption Geometry Comparison

property/geometry	Au–NCS[a]	Au–SCN[b]	Au–SCN–Au[c]
E_{Fermi} (eV)	−5.873	−6.288	−6.273
$E_{Fermi-Au}$ (eV)[d]	−5.920	−6.742	−7.763
Au−S (Å)		2.425	2.560
Au−N (Å)	2.164		2.325
S−C (Å)	1.583	1.644	1.627
C−N (Å)	1.204	1.182	1.195
ΔAu (Å)[e]	0.16	0.27	0.01
∠AuSC (deg)		104.3	84.2
∠SCN (deg)	177.7	174.4	171.3
∠AuNC (deg)	149.5		105.8
q_S (e)[f]	−0.10	0.12	0.28
q_C (e)	−0.06	−0.03	−0.08
q_N (e)	−0.49	−0.35	−0.36
q_{Au} (e)	0.04	−0.07	−0.02/0.11

[a] Au−NCS with −1 e charge is shown. [b] Au−SCN with 0 e charge is shown. [c] Au−NCS−Au with +1 e charge is shown. [d] The Fermi energy of the Au(111) slab before SCN adsorption [e] The vertical distance the Au atom moves after SCN adsorption. [f] The Mulliken population charge calculated for the atom. For Au, the table shows the charge on Au atoms closest to the S or N atom.

At −0.30 V (−1 e), the adsorption energy for the flat geometry is positive, which indicates that this configuration is unstable at this potential. The adsorption energy of both Au−NCS and Au−SCN is negative, and the difference between them is only 0.004 eV, which is too small to decide which geometry is more energetically favored. Thus, both geometries are expected to form on the surface at this potential.

As the potential is raised to 0.53 V (0 e), all the adsorption energies become negative, indicating that all three geometries are stable. Table 3 shows that the S-bound configuration is the most stable geometry, with the adsorption energy some 0.35 eV lower than that for the N-bound form and 0.64 eV lower than that for the bridging configuration. Thus, at this potential, S-bound adsorption of SCN is expected to dominate while N-bound and bridging structures are possible.

At a potential of 1.55 V (1 e), the Au−SCN−Au geometry is now most energetically favored and is 1.454 eV lower than that of the S-bound form and 2.603 eV lower than that of the N-bound. With such low adsorption energy, bridging SCN should dominate at this potential.

Shown in Figure 4 are the side and top views of the most stable adsorption geometries of SCN on the Au(111) surface with different external charge: (a) Au−NCS with −1 e charge, (b) Au−SCN without charge, and (c) Au−SCN−Au with +1 e charge adsorption. The geometric properties of these three configurations are given in Table 3.

III.B.3.(2). Interaction between SCN in the N-Bound Form and Au(111). At −0.3 V (with −1 charge), the most stable adsorption geometry for SCN is either N-bound or S-bound. Because of the (very) slight preference for N-bound and because S-bound will be discussed in the next section, we focus here only on the N-bound form. The calculation suggests that N-bound SCN is adsorbed at an atop site on the Au(111) surface. By fixing the geometry, we find that the adsorption energy at a 3-fold hollow site is some 0.114 eV higher (calculation not shown). The ∠AuNC angle is found to be 149.5°, and the ∠SCN angle is 177.7°. The Au−N bond length is calculated to be only 2.164 Å, and the Au atom directly contacting N atom moves 0.16 Å upward, suggesting a strong interaction between the surface and the molecule.[57] Compared with free SCN with −1 e charge in Table 1, the S−C bond contracts by 0.048 Å while

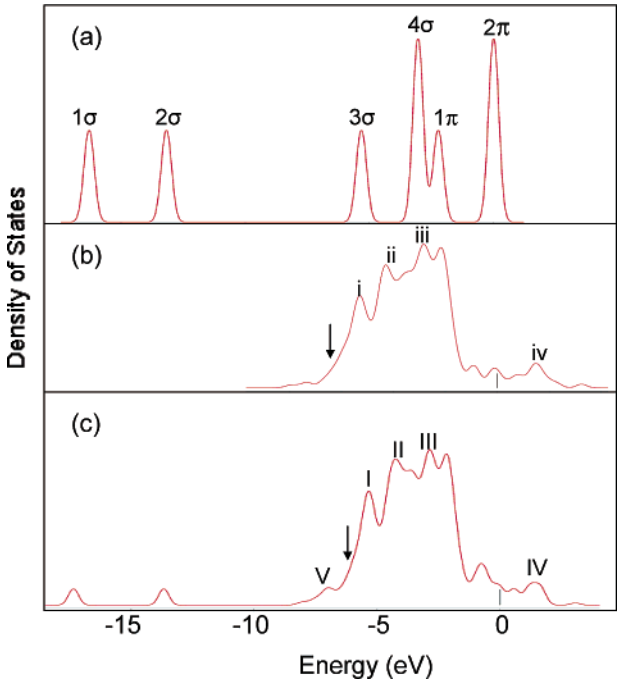

Figure 5. Density of states comparison for (a) free SCN without charge, (b) Au(111) with −1 e charge, and (c) SCN adsorption on the Au(111) surface via N end with −1 e charge. The arrows indicate the Fermi level.

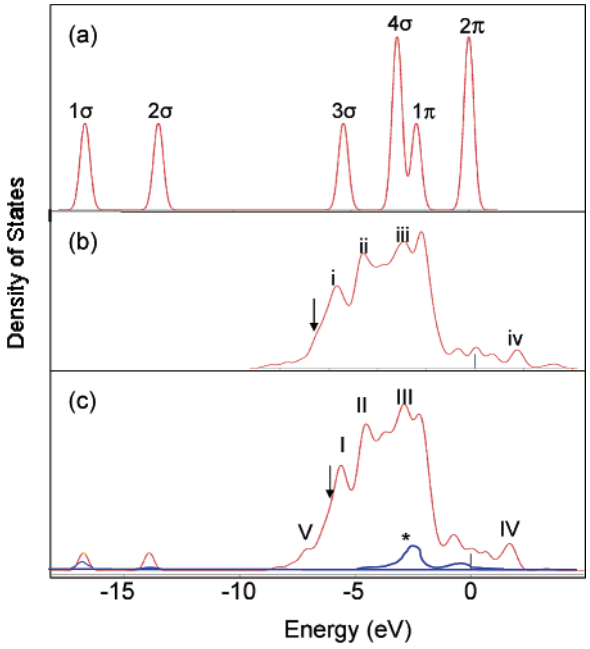

Figure 6. Density of states comparison for (a) free SCN without charge, (b) Au(111) without charge, and (c) SCN adsorption on the Au(111) surface via S end without charge. The arrows indicate the Fermi level. The blue inset in (c) is the N atomic density of states for SCN in this system.

the C−N bond increases slightly, which coincides with the formation of an Au−N bond. Substantial negative charge remains on N (−0.49 e), consistent with the calculation of the free anion described above.

Further insight into the association of N-bound SCN to Au(111) comes from the density of states (DOS), and results for free SCN, Au(111) surface with −1 e charge, and the adsorption system with −1 e charge are shown in Figure 5.

In Figure 5a, six orbitals are observed for the free SCN molecule: 1σ, 2σ, and 1π at −16.277, −13.166, and −2.242 eV are the bonding orbitals; 3σ, 4σ, and 2π at −5.326, −3.045, and −0.003 eV are the antibonding orbitals. Because in the software we are using the zero of energy for molecules is defined as the level of highest occupation and is not referenced to vacuum, only the sequences and the relative energy are under investigation. The order of the levels is in agreement with that found in other calculations.[29]

Panels b and c of Figure 5 show the DOS of the Au(111) slab without and with SCN adsorption with a −1 e charge. A comparison of panels b and c of Figure 5 shows that the energy of the Fermi level of the system increases from −5.920 to −5.873 eV with the presence of SCN, as indicated by the arrows. This 0.047 eV positive shift of Fermi level is associated with increased electron density on the surface due to charge transfer between the thiocyanate and the Au(111) structure.

The lowest two peaks in the DOS of the adsorption system (Figure 5c) at −17.331 and −13.669 eV originate from the negative shift of the SCN 1σ and 2σ orbitals. Compared with bare Au, a new peak, V, appears at − 7.070 eV, which originates from the 3σ orbital of SCN. On the basis of the atomic density of states analysis, the N atom contributes most to this state (52%) in the adsorption system while the 3σ orbital is mostly composed of S atoms (67%) in free SCN molecules. This difference indicates the strong interaction between the N atoms and the surface Au atoms. The features of the Au DOS otherwise exhibit only slight shifts on adsorption of SCN.

III.B.4. Interaction between SCN in the S-Bound Form and Au(111). The calculation indicates that S-bound adsorption is considerably more stable than the other two adsorption geometries without imposition of an external charge. In case of S-bound adsorption without external charge, we find that the energy of adsorption on the atop site is 0.364 eV lower than on the hollow site, which is different from the adsorption geometry calculated for SCN on a Ag cluster.[2] In our calculation, the first layer is allowed to relax upon SCN adsorption, and the Au atom directly contacting the S atom shifts up by 0.27 Å out of the plane. We note that ex situ STM images of SCN on Au(111) exhibit a complex pattern that was associated with Au reconstruction.[53] The calculated ∠AuSC and ∠SCN angles are 104.3° and 174.4°, respectively, which suggests that S-bound SCN tilts more than the N-bound form. The calculated Au−S bond length is 2.425 Å, which is close to that found in $Au(SCN)_2^-$ (2.468 Å).[58] Upon adsorption, the S−C bond elongates by 0.048 Å, while the C−N bond contracts by 0.016 Å. The calculated +0.12 e charge on the S atom and −0.07 e on the Au atom below it indicates electron donation from S to the Au surface.

III.B.4.(1). Density of States. Figure 6 shows the density of states for (a) free SCN, (b) the uncharged Au(111) surface, and (c) SCN adsorption on the Au surface without external charge. The DOS of free SCN in (a) has been discussed above. As the arrows indicate, the Fermi level of the adsorption system shifts positively from −6.742 eV in the case of bare Au(111) to −6.288 eV, which indicates the electron transfer between SCN and the surface. The lowest two peaks around −16.772 and

(57) Lambropoulos, N. A.; Reimers, J. R.; Hush, N. S. *J. Chem. Phys.* **2002**, *116*, 10277−10286.

(58) Muir, J. A.; Muir, M. M.; Arias, S. *Acta Crystallogr., Sect. B* **1982**, *38*, 1318−1320.

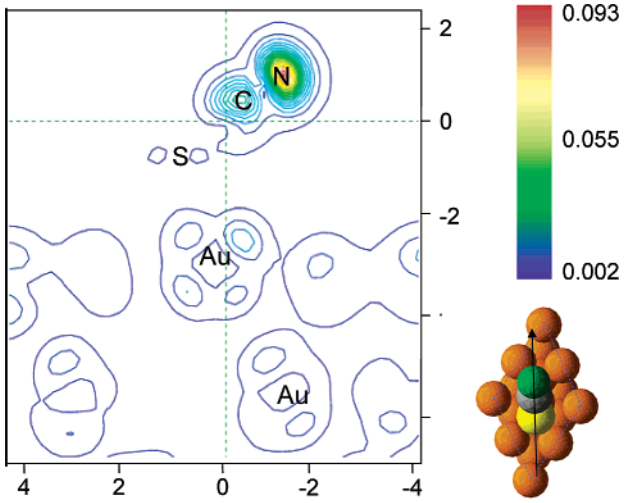

Figure 7. Charge-density contour for SCN adsorption on the Au(111) surface via the S atom without external charge at $E = -2.544$ eV. The plane of the plot, shown schematically at the right corner of the figure, is perpendicular to the surface and contains the center of S, C, and N atoms. The plot dimension is given in Å. The unit of charge density is e/Å^3. Au, S, C, and N atoms are represented by orange, yellow, gray, and green circles, respectively.

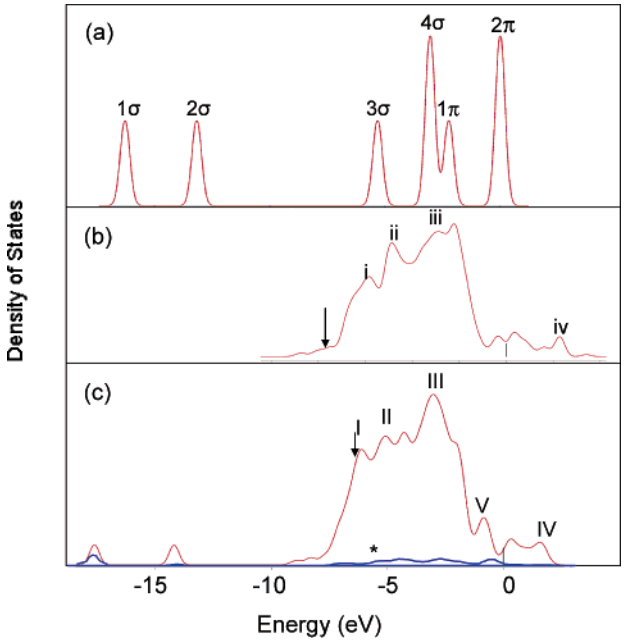

Figure 8. Density of states comparison for (a) free SCN without charge, (b) Au(111) with 1 e charge, and (c) SCN adsorption on the Au(111) surface via both N and S ends with 1 e charge. The arrows indicate the Fermi level. The blue inset in (c) is the N atomic density of states.

−13.915 eV originates from the negative shift of the SCN 1σ and 2σ orbitals. A comparison of states between panels b and c of Figure 6 shows that all the Au-related states shift by ca. −0.5 eV, which agrees well with the large adsorption energy, −1.187 eV, found for SCN in this system.

Interestingly, a new peak V appears with the adsorption at −7.063 eV. From the atomic DOS analysis, this peak is composed of S atoms (52%), C atoms (22%), and Au atoms that are directly under the S (26%). The blue inset in (c) shows the N atomic density of states. Clearly, there is not much contribution from this atom.

III.B.4.(2). Orbital Charge-Density Contour. To understand the interaction between C and N atoms for subsequent reference to the Stark shift behavior, the orbital charge-density contour at −2.544 eV is shown in Figure 7. The choice of this energy is based on the position of the maximum in the N atomic density of states marked with a *, as shown in Figure 6c. This energy represents the lowest unoccupied orbital of the C−N bond. Little charge is observed in the S atom region, which indicates that orbitals on the S atom do not contribute at this energy. The first- and second-layer Au atoms exhibit similar charge-density contours, which suggests that any interaction between the Au surface and the antibonding C−N bond is not localized at this energy.

III.B.5. Interaction between SCN in the Bridge-Bound Form and Au(111). In the bridging configuration with the +1 e external charge, SCN is nearly parallel to the Au surface with S atom on an atop site and N atom near a bridging site. The ∠SCN angle is 171.3°; the deviation from linearity presumably helps to facilitate interactions with the surface through both ends of the molecule. The Au−N and Au−S bond lengths are 2.325 and 2.560 Å, respectively; both are somewhat longer than that found for either end-on geometry. Furthermore, the 0.28 e charge on the S atom, the −0.02 e charge on the Au atom contacting the S atom combined with the −0.36 e charge on the N atom, and the 0.11 e charge on the two Au atoms closest to the N atom indicate a complex electron transference between the SCN and the Au surface below. These patterns suggest that the positive charge accruing to the Au surface helps to pull the negatively charged N atom close to the surface. However, enough electron density remains on the surface to also stabilize the Au−S interaction. SCN donates electron density through its S end while more electron density is withdrawn through the N atom.

III.B.5.(1). Density of States. Figure 8 shows the density of states for free SCN, the Au(111) surface with +1 e charge, and SCN adsorbed on the Au surface with +1 e charge. The free SCN DOS shown in Figure 8a has been discussed above.

As the arrows indicate, the energy of the Fermi level increases from −7.763 eV on the bare Au(111) surface to −6.273 eV after the SCN adsorbs in the bridging geometry on the surface. Relative to the two configurations discussed above, this large 1.490 eV positive shift of the Fermi level suggests the presence of considerable electron donation from the SCN to the Au surface, consistent with the extra positive charge in the system. Upon adsorption, the 1σ and 2σ orbitals of SCN shift more than −1 eV and settle at −17.619 and −14.698 eV, respectively. This large negative shift indicates the stronger interaction between SCN and the Au atoms below.

The ca. −0.2 eV shifts of all Au-related states in the DOS is consistent with the stabilization of SCN on the surface. Around the Fermi level, analysis of the DOS shows substantial contributions from S, C, N, and Au atoms, indicating that all of these atoms participate in bonding between SCN and the surface.

III.B.5.(2). Orbital Charge-Density Contour. Figure 9 shows the orbital charge-density contour of SCN in the bridging adsorption geometry on the Au(111) surface at an energy of −5.455 eV. The contour is chosen along the SCN bond as shown in the lower right of Figure 9. This energy is chosen because it is the energy of the lowest unoccupied N-based states of SCN. This energy is marked with a * in Figure 8c, where the blue line shows the N atomic density of states. The contour shows that most of the electron density at this energy is

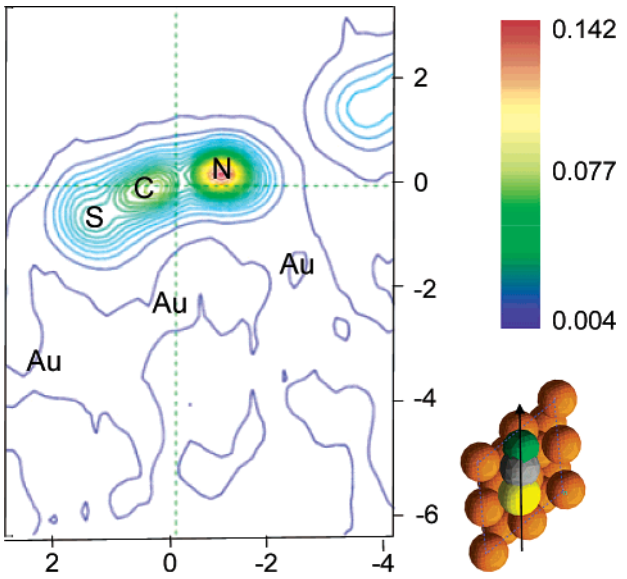

Figure 9. Charge-density contour for the SCN flat adsorption on the Au(111) surface with 1 e external charge at $E = -5.455$ eV. The cutting plane of the plot is indicated by the arrow at the right corner of the figure, which is perpendicular to the surface and contains the center of S, C, and N atoms. The plot dimension is given in Å. The unit of charge density is e/Å^3. Au, S, C, and N atoms are represented by orange, yellow, gray, and green circles, respectively.

accumulated between the C and N atoms, with a smaller amount on the S. There is little charge density on the Au surface. Interestingly, the contour shows that the S, C, and N are all bonding at this energy.

IV. Discussion

The measurements and calculations reported above provide considerable insight into the mechanism of thiocyanate adsorption on the Au surface. In particular, both results strongly support the fact that the adsorption geometry of thiocyanate changes with potential. Both the SERS and the DFT calculations show that SCN exhibits a behavior far richer on Au than was previously realized. To our knowledge, this is both the first experimental and theoretical establishment of a bridging geometry for SCN on Au. This is also the first time a negative Stark shift has been reported for this adsorbate.

IV.A. Change of Adsorption Geometry with Potential. Both the SERS measurements and calculations show the presence of three different adsorption geometries for SCN between 0.0 and 1.2 V. At the low potentials ($E \leq 0.4$ V), the C−N stretch modes of both N-bound and S-bound SCN were observed, while that of the N-bound is only the shoulder of the S-bound. This indicates that both end-on geometries are stable at low potentials, a result which is reinforced by the small differences between the calculated adsorption energies in the two geometries with −1 e external charge. When SCN is adsorbed through only the N atom, the calculation shows that the orbitals (both HOMO and LUMO) around the Fermi level are characteristic of bonding between the N atom and the Au surface. This behavior is to be contrasted with the apparent stability of sulfate on an Au cluster, where the tripod orientation of this molecule was found to be stable at all potentials examined.[45]

Table 2 also shows the trends in adsorption energy for each of the different binding geometries. For both the S-bound and the bridging configuration, the trend is toward more stable association with the Au surface at more positive potentials. For the S-bound form, there is little overlap between the S atom and the Au surface at −1 e charge, but this overlap increases as the surface charge moves from −1 e to 0 and +1 e. The origin of this increase in overlap is the movement of the Fermi level of the Au to lower energies as charge is removed, as shown in Table 3. Indeed, the lower-energy 3σ level of the free SCN is more centered on S,[28] and as the Fermi level moves to lower energies, there is increased interaction between this atom and the Au surface.

Table 2 shows that the trend in adsorption energy for the N-bound form is opposite that found for the other two geometries. In particular, the N-bound form is more stable at −1 e charge than at either 0 or +1 e. The origin of this behavior likely reflects the change in Fermi energy at −1 e charge. Here, the Fermi level overlaps with orbitals where N interacts with the Au surface. The orbitals with substantial N character, such as the 4σ level, are destabilized relative to the S-rich levels. As the charge on the surface becomes more positive, the Fermi level moves to lower energies, away from these orbitals, and the direct Au−N interaction decreases.

In the bridge-bound case, the negative charges found on both the S and N atoms in the anionic calculation clearly suggest that the molecule will be stabilized at positive potentials. The bridge-bound SCN is much more stable than the other two end-on geometries because of the strong interactions between both ends and the Au surface. Furthermore, calculation results suggest that the S−C−N angle bends most in the bridge geometry, which may explain the abrupt appearance of δ(NCS) mode at 0.9 V as the bridge form is stabilized on the surface.

As the potential is returned to more negative values, the SERS reveals that considerable intensity associated with the SCN molecule in the bridging configuration remains even down to 0.0 V. Since the calculation suggests that the bridge geometry is unstable at low potentials, remaining intensity in the $\nu_{Au-NCS-Au}$(C−N) mode is likely due to a kinetic effect. We note that holding the potential at 0.0 V for 2 h results in the complete disappearance of the $\nu_{Au-NCS-Au}$(C−N) mode and the recovery of S-bound and N-bound forms.

IV.B. Stark Effect of ν(C−N). In addition to showing the presence of different SCN adsorption geometries at different potentials, the SERS measurements also show that the Stark shift of the C−N stretch is dependent on both potential and adsorption geometry. The C−N stretch in the S-bound form exhibits a positive Stark shift, albeit with two different slopes depending on potential, while the C−N stretch in the bridge-bound form exhibits a negative Stark shift.

The positive potential dependence of ν_{Au-SCN}(C−N) has been studied extensively below 0.8 V.[17] It is found that the exact value of $d\nu_{CN}/dE$ depends strongly on both the surface nature and the techniques used. In particular, while potential-difference FTIR, SERS, and ATR IR measurements all give a Stark slope of between 10 and 16 cm^{-1} V^{-1}, IR-SFG spectroscopy revealed a much larger slope of 40 cm^{-1} V^{-1}. Our observation of two slopes depending on potential possibly provides an explanation for the different slopes observed with different techniques.

The Stark shift reflects the electric field experienced by the bond in question. Since the electric field decreases rapidly away

from the surface in the electrochemical environment,[59,60] the value of the Stark slope may also provide information about the distance between the bond and the surface. In the low potential region (0.0 V $\leq E \leq$ 0.8 V), calculations show that SCN adsorbs on the surface with an angle ∠AuSC of 104° and SCN is tilted 40° with respect to the Au(111) surface. A small Stark slope, 12 cm^{-1} V^{-1}, is observed. In the high potential region (0.8 V $\leq E \leq$ 1.2 V), the SCN must be in the process of reorienting from strictly S-bound to bridging. One consequence of this reorientation is that the N atom will become much closer to the Au surface. Consequently, the C−N bond will experience a stronger field, and this will result in a larger Stark slope. The experimental value 30 cm^{-1} V^{-1} reflects the closer approach of the C−N bond to the surface.

In the Supporting Information, we develop a simple point-dipole model, which gives the change in distance required to yield the different Stark slopes observed. In this model, the change in distance, Δz, is

$$\Delta z = \kappa^{-1} \ln(\delta_2/\delta_1) \tag{5}$$

where δ_2 and δ_1 are the two Stark slopes and κ^{-1} is the calculated Debye length for the double layer. The Stark slope δ_1 and δ_2 are 12 and 30 cm^{-1} V^{-1}, respectively, while κ^{-1} is 0.96 nm. This gives a $\Delta z = 0.88$ nm. This number is clearly larger than the real one since the molecular dimensions are ca. 0.45 nm. The model reflects the inadequacy of the point-dipole approximation to account for a phenomenon that clearly depends on the degree of coupling of the molecule with the surface, the nature of the C−N bond, and the interaction of the molecule with the double layer.

We now examine the origin of the different signs for the Stark slopes between the S-bound and bridging configurations. As the potential is moved to more negative values, electron density increases in the LUMO of the SCN adsorbate. Because the Stark effect in question relates to the C−N stretch, we examine in particular the lowest unoccupied orbital containing N character. In the case of the S-bound form, Figure 7 shows that this LUMO is strongly antibonding. This means that as electron density in this orbital is increased, the C−N bond becomes weaker, and consequently, the C−N stretching frequency should decrease, as is experimentally observed. This yields a positive Stark shift.

In the case of the bridging SCN, the lowest unoccupied orbital containing N atomic character is shown in Figure 9. This orbital is clearly a bonding-type level, which arises because of the strong interactions between both the N and the S of the SCN moiety. As the potential decreases, the Au surface becomes more negative, the electron density in the bonding orbital increases, and the C−N bond becomes stronger. Thus, the stretching frequency increases as the potential decreases, and a negative Stark slope is observed.

V. Conclusion

Thiocyanate adsorption on the Au surface is studied by potential-dependent SERS and detailed DFT calculations. Both experiment and calculation show that thiocyanate adsorbs in three different geometries as the potential changes: both end-on adsorption via N and S is preferred at low potentials, S end-on adsorption is dominant around E_{pzc}, and bridge geometry is most energy-favored at high potentials. End-on adsorption is found to be most stable on top site instead of the hollow sites on the Au surface, which is due to the out-of-plane shift of the Au atom directly contacting the thiocyanate. The origin of the different geometries found at different potentials likely relates to the overlap of the Fermi level of the metal with orbitals on the SCN adsorbate. At low potentials, the higher Fermi energy allows overlap with N-containing orbitals, while at higher potentials, the Fermi energy is too low, and overlap with S-centered orbitals is favored. This model of potential-dependent adsorption geometries has predictive utility, and we are in the process of examining its consequences for other adsorbates.

The dependence of the C−N stretch frequencies on potential is also examined. For both N and S end-on adsorption, the Stark slope is positive, and the magnitude found here agrees with previous work.[14] However, two different values of the Stark slope are found for the S-bound geometry: a small slope in the low potential region (0.0 V $\leq E \leq$ 0.8 V) and a larger one at high potentials (0.8 V $\leq E \leq$ 1.2 V). The origin of these different slopes likely reflects reorientation of the molecule at the higher potentials. For the bridging geometry, the Stark slope is negative. The calculations suggest that the origin of this behavior resides in the bonding nature of the C−N-centered LUMO found for this geometry. By way of contrast, the C−N LUMO is antibonding for the end-on geometries.

These results suggest that the adsorbate−electrode interaction depends on not only the nature of both the adsorbate and the electrode, but also on the applied potential and, hence, Fermi energy of the metal. That even a simple molecule like SCN can exhibit a rich chemistry on Au suggests that these behaviors might also be obtained in more complex systems.

Acknowledgment. X.L. thanks the Department of Chemistry for financial support in the form of a Carl Shipp Marvel Fellowship and the Chester W. Hannum Scholarship. This work was partially supported by National Computational Science Alliance (NCSA) under CHE030003 and utilized the NCSA Origin2000. The authors thank R. Strange and J. O. White of the Laser Laboratory in the Frederick Seitz Materials Research Laboratory at the University of Illinois for their assistance in Raman data acquisition. The Laser Laboratory is funded by Department of Energy Grant DE-FG02-91ER45439 through the Materials Research Laboratory at the University of Illinois. This material is based upon work supported by the U.S. Department of Energy, Division of Materials Sciences under Award No. DE-FG02-91ER45439, through the Frederick Seitz Materials Research Laboratory at the University of Illinois at Urbana-Champaign.

Supporting Information Available: Derivation of eq 5, SERS results between 0.8 and 0.0 V, and geometries (Cartesian coordinates) of all calculated slabs (PDF). This material is available free of charge via the Internet at http://pubs.acs.org.

JA0363112

(59) Weaver, M. J.; Zou, S. Z.; Chan, H. Y. H. *Anal. Chem.* **2000**, *72*, 1.
(60) Bard, A. J.; Faulkner, L. R. *Electrochemical Methods: Fundamentals and Applications*; John Wiley & Sons: New York, 1980.